

Cation mono- and co-doped anatase TiO_2 nanotubes: An *ab initio* investigation of electronic and optical properties

Mohamed M. Fadlallah^{1,*} and Ulrich Eckern^{2,†}

¹*Physics Department, Faculty of Science, Benha University, Benha, Egypt*

²*Institute of Physics, University of Augsburg, 86135 Augsburg, Germany*

Abstract

The structural, electronic, and optical properties of metal (Si, Ge, Sn, and Pb) mono- and co-doped anatase TiO_2 nanotubes are investigated, in order to elucidate their potential for photocatalytic applications. It is found that Si doped TiO_2 nanotubes are more stable than those doped with Ge, Sn, or Pb. All dopants lower the band gap, the decrease depending on the concentration and the type of dopant. Correspondingly, a redshift in the optical properties for all kinds of dopings is obtained. Even though a Pb mono-doped TiO_2 nanotube has the lowest band gap, this system is not suitable for water splitting, due to the location of the conduction band edge in this system, in contrast to Si, Ge, and Sn mono-doped TiO_2 nanotubes. On the other hand, co-doping of TiO_2 does not improve its photocatalytic properties. Our findings are consistent with recent experiments which show an enhancement of light absorption for Si and Sn doped TiO_2 nanotubes.

Keywords: nanotube, titania, metal doping, electronic and optical properties, density functional theory

* mohamed.fadlallah@fsc.bu.edu.eg

† ulrich.eckern@physik.uni-augsburg.de

I. INTRODUCTION

Titanium dioxide (TiO_2), also known as titania, has been widely studied as a promising material for many applications because of its low production cost, chemical stability, and non-toxicity [1–3]. Titania is useful for, in particular, solar cells [4], batteries [5], photochemical [6] and photocatalytic [7] applications, gas sensing [8], and hydrogen storage [9–11]. However, TiO_2 can only be activated by ultraviolet light due to its large band gap (3.0 eV for the rutile, and 3.2 eV for the anatase phase). Therefore, engineering the band gap [12–14] of titania in order to increase its photosensitivity for visible light is a major target in photocatalyst studies.

In recent years, various low-dimensional TiO_2 nanostructures have been prepared, such as thin films [15], nanoparticles [16, 17], nanowires [18, 19], and nanotubes [20, 21]. TiO_2 nanotube (TNT) arrays are most interesting for applications due to their large internal surface and highly ordered geometry [22–24]. The structural properties, stability and electronic structure of different TNT structures (anatase and lepidocrocite) have been discussed, e.g., in Ref. 25. All anatase nanotubes are semiconductors with direct band gaps while the lepidocrocite nanotubes are semiconductors with indirect gaps. In addition, anatase nanotubes were found to be most stable; their stability increases with increasing diameter [26–28]. The rolling of an anatase (101) sheet along the [101] and [010] directions has been used to build $(n, 0)$ and $(0, n)$ TNTs, respectively [29]. The experimental results show that the predominant peaks of anatase and rutile nanotubes are (101) and (110) [30, 31]. Recently, several mono- and co-doped TNTs have been synthesized, e.g., C [32], P [33], Co [34], Si [35], and Sn [36] mono-doped, as well as (C/N, F) co-doped [37] TNTs. On the other hand, doped TNTs have been studied theoretically only occasionally, e.g., N and B doping [38], C, N, S, and Fe doping [39], (N, S) co-doping [40], and nonmetal and halogen doping [41].

In the context of the present study, we note that an improvement of the photocatalytic properties of bulk TiO_2 has been observed experimentally [42, 43] and calculated theoretically [44, 45] for Si doping. Other dopings (Ge, Sn, Pb) are also known to reduce the band gap in the rutile bulk system, while Sn and Pb doping slightly broadens the band gap in anatase TiO_2 [44]. Experimentally an improvement of photocatalytic properties was found for Sn doped bulk systems synthesized by the hydrothermal method [46]. TiO_2 thin films doped with Si [47], Sn [48], Pb [49], and Ge [50] have been prepared and investigated, gener-

ally showing an improvement of photocatalytic activity upon doping. With respect to TiO_2 nanotubes, a suitable doping with Si also improves the light absorption [35, 51]. Similar results have been found for Sn doping where, however, also a transformation from anatase to rutile is observed [36]. Thus, in the light of these previous experimental and theoretical studies, and in view of their potential high relevance for photocatalytic applications, we perform a systematic study of doping anatase TNT with group-IV elements, as a function of dopant concentrations; in addition, co-doping effects are also investigated.

In the following, after describing the methodology (section II), we investigate the effect of the mono-dopants (Si, Ge, Sn, Pb) on the structure and stability of $(n, 0)$ titania nanotubes (section III). Then we study the electronic structure of doped TNTs (section IV), followed by a discussion of the optical properties (section V). An application of this study is the splitting of water (section VI). We close our work with a brief summary (section VII).

II. METHODOLOGY

We apply density functional theory (DFT) employing the generalized gradient approximation (GGA) [52, 53] and the Perdew-Burke-Ernzerhof functional [54] as implemented in the SIESTA package [55]. The wave functions are expanded using a local atomic orbitals basis set; the energy cutoff is 300 Ry, and the Monkhorst-Pack k -meshes contain $1 \times 1 \times 12$ points. Structural relaxation is carried out with the conjugate gradient method until the net force on every atom is smaller than $0.04 \text{ eV}/\text{\AA}$. As we are interested in the properties of nanotubes, a rectangular supercell, $20 \times 20 \times L \text{ \AA}^3$, is used, where L is the length of the nanotube along the z axis. The distance between two neighboring TNTs, in x and y directions, is thus 20 \AA , which is sufficient to avoid any image interaction. Test calculations, changing the size of the supercell and the number of k -points, show the convergence of our results. Spin polarized calculations have also been performed for selected systems, but no modifications were found.

III. OPTIMIZED STRUCTURE AND STABILITY OF TiO_2 NANOTUBES

The total number of the atoms in the unit cell of a TNT is related to the number of atoms in one unit cell (48 atoms) in the surface layer. We use a supercell including two TNT unit

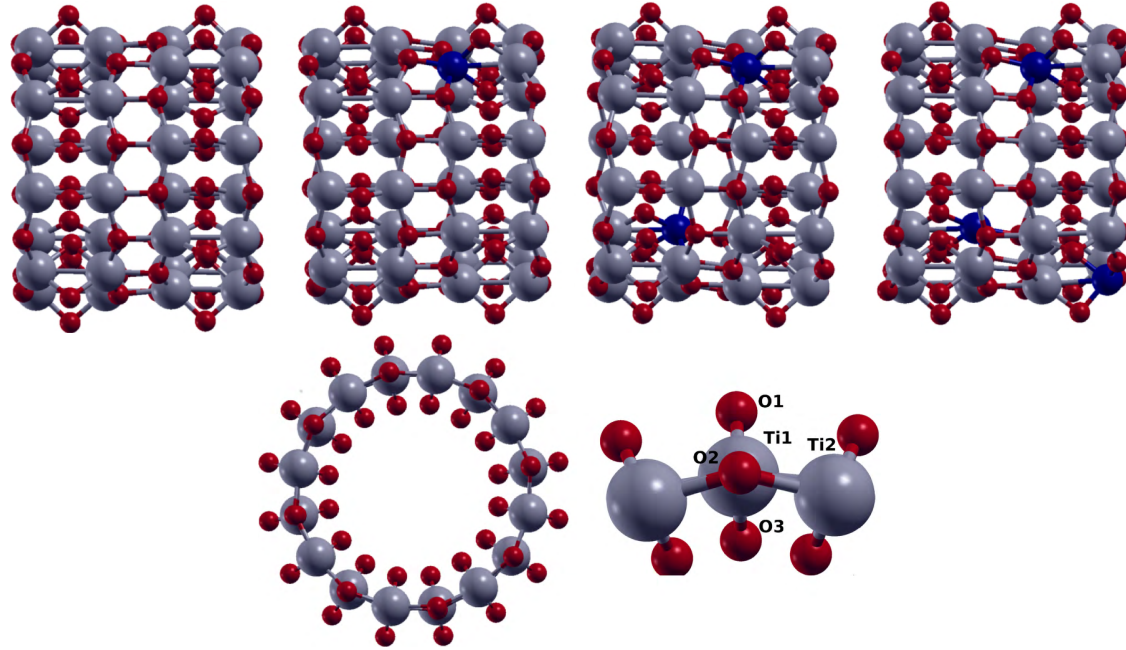


FIG. 1. Top part: Optimal configuration (side view) for pristine TNT, 1% doped TNT, 2% doped TNT, and 3% doped TNT (from left to right). Lower part: Top view of the pristine TNT (left) and detail of the wall (right). The indicated labels are discussed in the main text. Red, grey, and blue spheres represent O, Ti, and dopant atoms, respectively.

cells to study the effect of changing the doping concentration. Figure 1 shows the structure of two unit cells of (8, 0) TNT. The fundamental periodic of the TNT nanotube (along z direction) is 10.49 Å, which is only slightly larger than found in a previous study (10.12 Å) [28]. Concerning other geometric parameters, we find the inner diameter of the nanotube, cf. the lower part of Fig. 1, i.e., between an O3 and its opposite counterpart, to be given by 7.07 Å, while the distance between an O1 and its opposite counterpart is 12.05 Å; the diameter with respect to the Ti atoms is 9.51 Å, and the O1–O3 distance is 2.49 Å. The bond length Ti1–O1 (equal to Ti1–O3) is 1.84 Å, while the bond Ti2–O2 is slightly longer, 1.95 Å, in good agreement with previous works [28, 56].

Cation doping of the TNT is introduced by replacing Ti atoms by the dopants. Replacing one Ti by a metal dopant corresponds to $\sim 1.0\%$ dopant concentration. If two atoms are substituted, the doping concentrations will double, and so on. These dopant concentrations are comparable to those reported experimentally [57]. The dopant-dopant interaction was avoided due to the large distance between them (11 Å for 2%, and 8 Å for 3% dopant

concentrations). The optimized average bond lengths around the dopant atoms are listed in Tab. I. The bond length between the dopant atom and the O atom increases as the ionic radius of the dopant increases: Si, Ge, Sn, and Pb, with radii 0.40, 0.53, 0.69, and 1.19 Å, respectively. The ionic radius of Ti^{4+} is 0.61 Å.

The charge deficiency on the metal, estimated as the difference between electronic charge densities obtained with the Mulliken population analysis, is also given in Tab. I. The table shows that the charge transfer from the dopant atom to the surrounding O atom is rather high for Si and Sn, as compared to Ge and Pb. The formation energy of doped TNTs is used to investigate the stability of the structures. The formation energy (E_{form}) of the dopant atoms can be calculated as follows [58]:

Metal	Si	Ge	Sn	Pb
M–O	1.77	1.94	2.09	2.18
Mulliken charge	2.12	1.48	2.05	1.78
E_{form}	1.5	2.1	3.1	4.2

TABLE I. Bond lengths between dopant metal and oxygen, M–O (Å), Mulliken charge on dopants (e), and formation energy, E_{form} (eV), for doped TNT.

$$E_{\text{form}} = E_{\text{M–TiO}_2} + \mu_{\text{Ti}} - (E_{\text{TiO}_2} + \mu_{\text{M}}), \quad (1)$$

where $E_{\text{M–TiO}_2}$ and E_{TiO_2} are the total energies of the metal-doped TiO_2 and the pristine TiO_2 nanotube, respectively, while μ_{Ti} and μ_{M} denote the chemical potentials for Ti and the dopant; the latter are assumed to be equal to the energy of one atom in its corresponding bulk structure.

The formation energy depends on the growth conditions, which can be Ti-rich or O-rich [59]. For the Ti-rich condition, thermodynamic equilibrium is assumed for the Ti bulk solid phase, thus its chemical potential is fixed at μ_{Ti} , while the chemical potential of O is fixed by the growth conditions. Under the O-rich condition, O is assumed to be in equilibrium with O_2 molecules, thus the chemical potential of O is $\mu_{\text{O}} = \mu_{\text{O}_2}/2$. We present the formation energy under the O-rich condition, which is lower than for the Ti-rich condition. The stability of nanotubes with dopants is in the following order: Si, Ge, Sn, Pb. The behavior of the formation energies can be understood, to a large extent, in terms

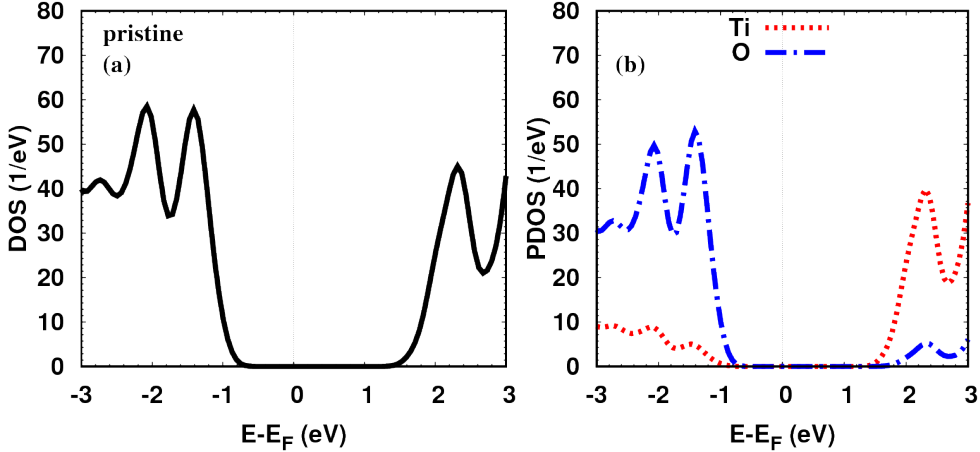


FIG. 2. (a) Density of states (DOS), and (b) partial density of states (PDOS) of the pristine TiO_2 (8, 0) nanotube.

of the dopant's electronegativity given by 1.90 (Si), 2.01 (Ge), 1.96 (Sn), and 2.33 (Pb). On the one hand, one notes that the formation energy of Si is smaller than that of the other dopants, corresponding to the fact that Si has the smallest electronegativity. On the other hand, the Pb formation energy is the largest, and so is its electronegativity. From this point of view, Ge and Sn doped TNTs are ‘out of order’, which can be related to the effect of electronegativity on the ionic radius, implying that the formation of Sn–O bonds is more favorable than Ge–O bonds. This behavior of formation energies and bond lengths is very similar to the behavior of the corresponding dopant in bulk TiO_2 [44].

IV. ELECTRONIC STRUCTURE

Figure 2(a) shows the density of states (DOS) for pristine titania nanotubes (8, 0). The band gap of the pure TNT is 2.21 eV, which is lower than the corresponding gap of bulk TiO_2 anatase [60] due to the well known shortcoming of the GGA. The Ti states dominate in the unoccupied states, while the O (p) states contribute mostly to the occupied states with a minor contribution to the unoccupied states, see Fig. 2(b). The DOS and PDOS (partial DOS) are very similar to the results obtained in Ref. 56.

The effect of Si doping on the electronic structure of TNT is shown in Fig. 3(a). As compared to the DOS of pristine TNT, the Fermi energy moves to higher energy; the band

gap is 1.80 eV for 1% doping, which is less than that of pristine TNT. When the concentration is increased to 2% and 3%, the Fermi energy shifts further upwards, but this shift is larger for 2% than for 3%. The band gap remains at 1.80 eV for 2%, and increases to 1.86 eV for 3% dopant concentration. This decrease of the band gap is consistent with the observed increase of optical absorption of TNT upon Si doping [35, 51, 61]. The shift of the Fermi energy is also seen in the Si PDOS, Fig. 3(b). The band gap in the Si PDOS is larger than the band gap in the DOS, indicating that the top of the valence band and the bottom of the conduction band are still dominated by O and Ti states, respectively: As is apparent from Fig. 2(b) in comparison with Figs. 3(a) and 3(b), the Si states are located well inside the valence band and the conduction band, and their contribution at the band gap edges is negligible (note the different scale in the PDOS plots). Nevertheless, a small downshift of the conduction band is found in comparison with pristine TNT for 1% doping, in good agreement with the results of Ref. 44 for the corresponding bulk system, while the valence band edge is unaffected. For higher concentrations, 2% and 3%, a shift of both band edges is observed. The Si states for 1% dopant contribute most strongly around 2.5 eV, and below -1 eV. For 2% and 3% concentrations, the contribution of Si states appears mostly around 1.8 eV, and below -1.6 eV.

Figure 3(c) shows that the Fermi energy is slightly shifted towards higher energy due to Ge substitution, as compared to pristine TNT, Fig. 2(a). The band gap is 1.86 eV, which is less than the band gap of pristine TNT but larger than that of Si doped TNT at the same concentration. The result for a Ge dopant concentration of 2% is very similar to 1%. However, a doping of 3% shifts the Fermi energy upwards with an increase in the band gap to 1.96 eV. These Fermi energy shifts can be explained using the PDOS of Ge as shown in Fig. 3(d). Similar to Si doping, see above, the PDOS has a band gap larger than the DOS which indicates that the edges of the bands are related to the host atoms. The Ge states have a noticeable contribution at 2.5 eV and below -0.4 eV for 1% and 2% concentrations, while for 3% they are located above 1.8 eV and below -2 eV. For Ge doping, the DOS change is very similar for 1% and 2%; in both cases, an upshift of the band edges is found, in contrast to Ge doping of bulk TiO_2 [44].

For Sn doped TNTs, Fig. 3(e), which overall is very similar to Si doping, the Fermi energy increases to higher energy as compared to pristine TNT, with a band gap of 1.93 eV, which is larger than the gap of Si and Ge doped TNT at the same concentration. When

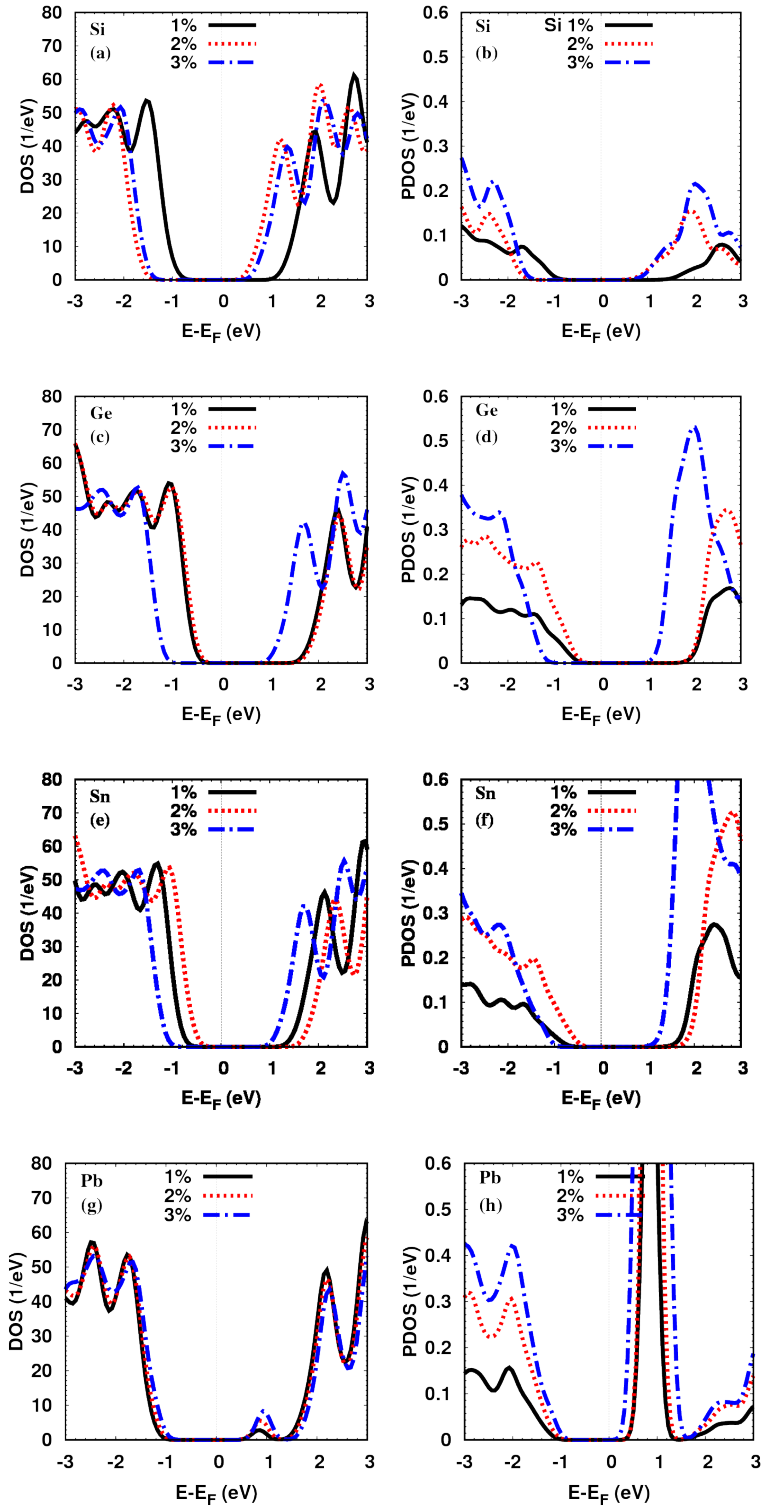


FIG. 3. Density of states (DOS) and partial density of states (PDOS) for Si (a, b), Ge (c, d), Sn (e, f), and Pb (g, h) doped TNT; DOS (left) and PDOS (right).

the concentration increases to 2%, the DOS becomes very similar to the DOS of 2% Ge doping, i.e., the Fermi energy moves to lower energy as compared to 1% Sn. Increasing the Sn dopant to 3% shifts the Fermi energy towards higher energy as compared to 1% and 2% Sn concentrations. The band gap decreases for 2% Sn to 1.86 eV, and does not change for 3% Sn, and thus is similar to 1% Sn concentration. The computed reduction of the band gap through Sn doping is in good agreement with the corresponding experiment where an enhancement of light absorption is found [36]. The contribution of Sn states is illustrated in Fig. 3(f); it is similar to Ge doping at the corresponding concentrations. The contribution of dopant states for Sn in the conduction band is higher than that of Si and Ge in the same band.

Within the mono-doped series, we finally consider Pb, for which we find a small shift of the Fermi energy to higher energy as compared to the previously studied dopants, see Fig. 3(g). A distinct effect of the Pb dopant is the creation of states below the conduction band at 0.9 eV. These states reduce the band gap to 1.56 eV, which is the lowest band gap in comparison to the other dopants at 1% concentration. Increasing the concentration of Pb, the shift of the Fermi energy increases slightly towards lower energy. In addition, the increase of doping concentration decreases the band gap slightly to 1.50 eV, and 1.44 eV for 2% and 3%, respectively. The PDOS shows that the additional states derive from the Pb states, see Fig. 3(h). The location of Pb states in the conduction band hardly changes with increasing doping, in contrast to what we observed for the other dopants; in addition, this contribution to the conduction band is larger. However, the Ti states also have visible contributions at the same energy.

Turning to co-doped TNT, the doping concentration is 2% for two different kinds of substitutional atoms, and 3% for two atoms from the same kind plus one doped atom from another kind. Figure 4(a) shows the effect of Si/Ge co-doping on the electronic structure. The DOS of (Si, Ge) co-doping is very similar to Si mono-doped TNT at 2% concentration with a large band gap of 1.92 eV. When the concentration increases to 3% (whether (2Si, Ge) or (2Ge, Si)) co-doping the Fermi energy moves towards higher energy as compared to (Si, Ge) co-doping; the band gap slightly increases to 1.98 eV for (2Ge, Si) only. For Si/Sn co-doping, the Fermi energy shifts towards higher energy, more strongly than for Si and Sn mono-dopants (Fig. 4(b)); the band gap (1.98 eV) is also larger than for mono-dopants. As compared to (Si, Sn) co-doping, the increase of the Si concentration in the co-dopants

narrows the band gap to 1.86 eV. The top of the valence band shifts towards higher energy, but the bottom of the conduction band does not change. For (2Sn, Si) the only change is an upward shift of the Fermi energy. For Si/Pb co-doped TNT, the effect of the Pb dopant is dominant in the DOS, as shown in Fig. 4(c). The DOS of the (Si, Pb) co-doped system is very similar to the DOS of Pb mono-doped TNT which is characterized by Pb dopant states below the conduction band. The band gap for this co-doping, 1.50 eV, is larger than the band gap for Pb mono-doping. For substitutional (2Si, Pb) co-doping, the band gap remains unchanged. The Fermi energy is shifted towards higher energy, and the Pb states below the contribution band have a different shape, as compared to the (Si, Pb) co-doped structure. Concerning (Si, 2Pb) co-doping, the Fermi energy shift is larger than for (2Pb, Si) co-doping, and the band gap has a value similar to 3% Pb mono-doping, i.e., 1.44 eV.

Figure 4(d) shows the DOS for Ge/Sn co-doping. The Fermi energy moves towards higher energy as compared to Ge and Sn mono-doping; the band gap of (Ge, Sn) co-doping is similar to 1% Ge mono-doping. The Fermi energy in the case of (2Ge, Sn) shifts to lower energy, with a smaller band gap, 1.74 eV, as compared to (Ge, Sn). The (2Sn, Ge) co-doping Fermi energy shift is less than for (2Ge, Sn) co-doping, but the band gap is the same. With respect to Ge/Pb co-doping, Fig. 4(e), the DOS is very similar to the DOS of Pb mono-doping, and does not depend on the concentration of the co-dopant. Only a slight change in the band gap is found for (2Pb, Ge), the gap being 1.38 eV, as compared to (Ge, Pb) and (2Ge, Pb) where the gap is 1.50 eV. The last co-dopant in this study is Sn/Pb, see Fig. 4(f). The effect of this co-dopant on the DOS at different concentrations is very similar to the effect of (Si, Pb). The Fermi energy shift is small for (Sn, Pb) and (2Sn, Pb) in comparison to the (Si, Pb) and (2Si, Pb) systems, however, the shift is large for (2Pb, Sn) in comparison to (2Pb, Si). The band gap of Sn/Pb at different concentrations of Sn is similar to the gap of Si/Pb at the corresponding Si concentrations, while the gap for (2Pb, Sn) co-doping, 1.38 eV, is less than the gap for (2Pb, Si) co-doping.

V. OPTICAL PROPERTIES

The optical properties of a semiconductor photocatalyst are closely related to its electronic structure. The shift of the Fermi energy towards higher energy in combination with a decrease of the band gap for all mono-dopants as compared to pristine TNT, see Fig. 3, leads

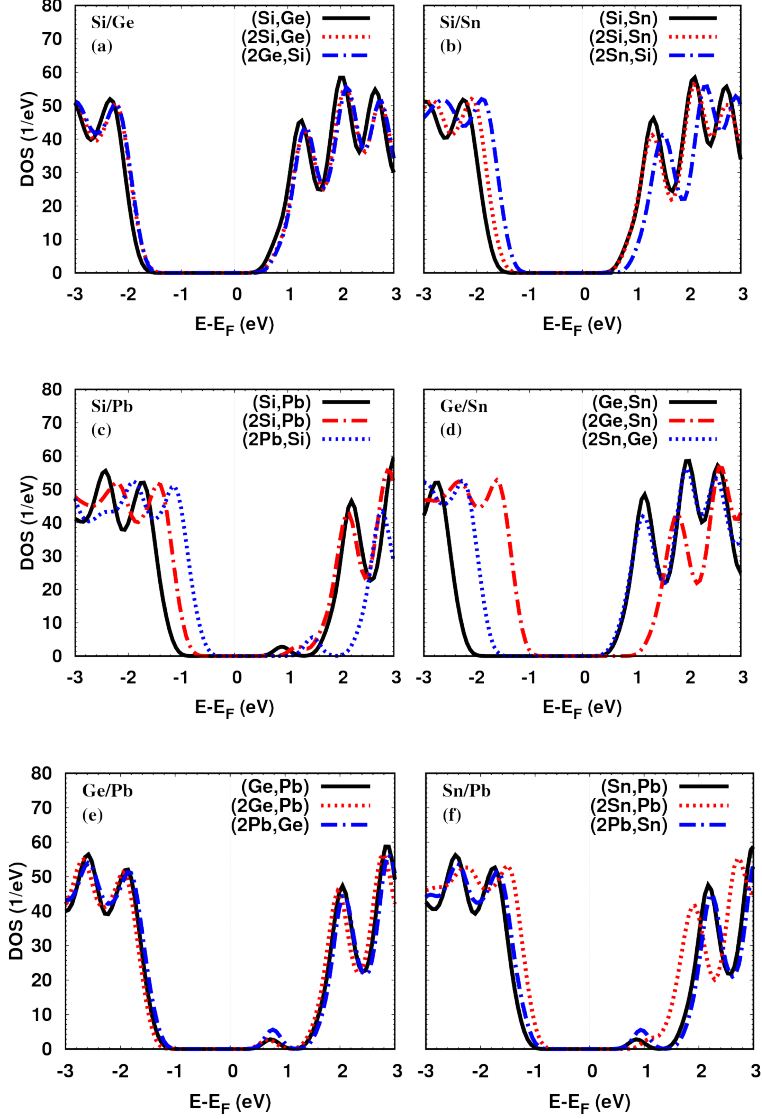


FIG. 4. Density of states (DOS) for Si/Ge (a), Si/Sn (b), Si/Pb (c), Ge/Sn (d), Ge/Pb (e), Sn/Pb (f) co-doped TNTs.

to a redshift of the optical absorption edge. This redshift depends on the kind of dopant and the concentration. The redshift for Pb and Sn mono-doped TNT is, in contrast to Pb and Sn doped bulk anatase TiO_2 [44], due to the difference in the geometry, electronic structure, and the interaction between dopant and neighboring Ti and O atoms. The redshift is also noticeable in co-doped TNT, see Fig. 4.

The optical absorption is related to the complex dielectric function $\varepsilon(\omega) = \varepsilon_1(\omega) + i\varepsilon_2(\omega)$, with ω the frequency. The imaginary part is calculated from the momentum matrix

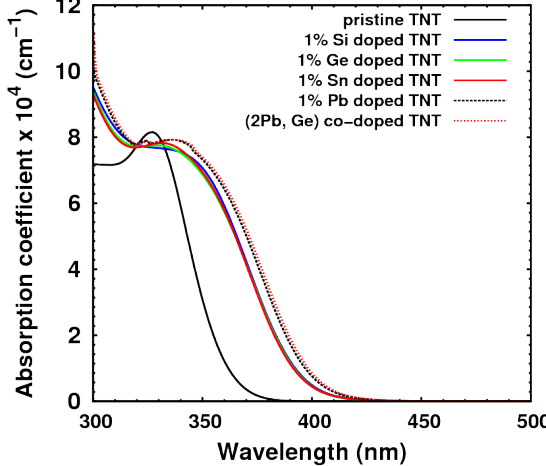


FIG. 5. Absorption coefficients of pristine, mono- and co-doped TiO_2 nanotubes.

elements between the occupied and unoccupied states, and the real part subsequently from the Kramers-Kronig relation. The absorption coefficient then is given by [62]

$$\alpha(\omega) = \sqrt{2}\omega \sqrt{\sqrt{\varepsilon_1^2(\omega) + \varepsilon_2^2(\omega)} - \varepsilon_1(\omega)}. \quad (2)$$

A “scissors operation” [63–65] of 1.0 eV, which corresponds to the difference between the calculated and the experimental gap (3.2 eV) for pristine TNT, is also used for the doped system.

A pristine TiO_2 nanotube can only absorb the narrow UV light (370 nm), but shows no absorption for visible light, see Fig. 5. The calculated optical absorption spectra for all mono-doped TNTs show absorption in the visible-light region, namely in the range 380 – 410 nm. Also, a redshift is apparent for all mono-doped TNTs, consistent with the earlier discussion.

VI. APPLICATION: WATER SPLITTING

The improvement of the visible light activity of TiO_2 is very important for water splitting (H production) [66, 67]. The calculations of the conduction band edge (CBE) and the valence band edge (VBE) [58] show that the CBE of TiO_2 is located at –0.29 eV, above the water reduction (H^+/H_2) level, while the VBE is located at 1.65 eV, below the water oxidation ($\text{H}_2\text{O}/\text{O}_2$) level [68]. These band edges are measured with respect to the normal hydrogen electrode potential of the reduction and oxidation levels of water. The oxidation level of water ($\text{H}_2\text{O}/\text{O}_2$) is located at 1.25 eV, and the reduction level (H^+/H_2) at 0 eV.

	pristine	Si dopant			Ge dopant			Sn dopant			Pb dopant		
		1%	2%	3%	1%	2%	3%	1%	2%	3%	1%	2%	3%
CBE	-0.29	-0.08	-0.08	-0.07	-0.11	-0.09	-0.07	-0.15	-0.1	-0.12	0.03	0.07	0.11
VBE	2.9	2.94	2.94	2.93	2.97	2.95	2.93	3.05	2.96	3.04	2.53	2.43	2.33

TABLE II. Conduction band (CBE) and valence band (VBE) edges, both in units of eV, of pristine TNT and doped TNTs for different concentrations. The energies are given with respect to the normal hydrogen electrode (NHE) potential; cf. the related discussion in section 5 of [41]. Note that 0 eV (NHE) corresponds to -4.5 eV (vacuum).

Table II shows that Si, Ge, and Sn mono-doping of TNTs improves the photocatalytic properties, at any concentration. However, the CBE value is too high compared to the reduction level of water, hence Pb doped TNTs are useful for hydrogen production despite the fact that they have the lowest band gaps among the mono-dopants. The low-concentration Si and Ge doped structures show a better efficiency than for high concentration. In contrast, for bulk TiO_2 anatase only Ge doping improves the photocatalytic properties [44]. We do not present the co-doping results here because all of them have CBEs around -2 eV, which is higher than the reduction level of water, and the VBEs are higher than the oxidation level.

VII. SUMMARY

Density functional theory has been employed to study the structural, electronic, and optical properties of cation mono- and co-doped titania nanotubes (TNTs) at different doping concentrations. All mono-/co-dopants decrease the band gap of the TNT, similar to previous results [41]. For mono-dopants, Pb doped TNTs have the lowest band gap at the studied concentrations (1% to 3%) due to the presence of Pb states below the conduction band. The contribution of the dopant states in the conduction band increases as we move down the 4A group in the periodic table, i.e., from Si to Ge, Sn, and Pb. The decrease in the band gaps of mono-doped TNTs is accompanied by shifts in the Fermi energy towards higher energy. The band gaps of co-doped TNTs are smaller than those of Si, Ge, and Sn mono-doped TNTs at any concentration. The (2Pb, Sn) co-doped TNT has the lowest band gap of all mono- and co-doped TNTs. The influence of co-dopants can be understood, to a

large extent, in terms of a superposition of individual mono-dopant effect.

The study of optical properties illustrates that mono- and co-doped TNTs can absorb a wide range of visible light, in contrast to pristine TNT. This observation, consistent with recent experimental results, is related to the decrease of the band gap, and the shift of the Fermi energy. The Si, Ge, and Sn mono-doped TNTs at low concentration (1%) have a high ability to produce hydrogen in the water splitting process, their performance being clearly better than for pristine TNT. The band gap edge locations of Pb mono-doped and co-doped TNTs, however, prevent their use for this application.

ACKNOWLEDGMENTS

We acknowledge financial support by the German Research Foundation (DFG) through TRR 80.

- [1] T. Tachikawa and T. Majima, *Chem. Soc. Rev.* **39**, 4802 (2010).
- [2] C. C. Chen, W. H. Ma, and J. C. Zhao, *Chem. Soc. Rev.* **39**, 4206 (2010).
- [3] F. Spadavecchia, G. Cappelletti, S. Ardizzone, M. Ceotto, and L. Falciola, *J. Phys. Chem. C* **115**, 6381 (2011).
- [4] A. Motonari, J. Jinting, and I. Seiji, *Curr. Nanosci.* **3**, 285 (2007).
- [5] D. Deng, M. G. Kim, J. Y. Lee, and J. Cho, *Energy Environ. Sci.* **2**, 818 (2009).
- [6] T. Umebayashi, T. Yamaki, H. Itoh, and K. Asai, *Appl. Phys. Lett.* **81**, 454 (2002).
- [7] L. Y. Mu, J. J. Hyun, A. J. Hyung, J. Y. Sun, J. K. Ok, H. K. Seog, and K. B. Hoon, *J. Cer. Proc. Res.* **6**, 302 (2005).
- [8] J. Zhao, X. Wang, T. Sun, and L. Li, *Nanotechnology* **16**, 2450 (2005).
- [9] M. R. Hoffmann, S. T. Martin, W. Choi, and D. W. Bahnemann, *Chem. Rev.* **95**, 69 (1995).
- [10] M. Grätzel, *Nature* **414**, 338 (2001).
- [11] O. K. Varghese, D. Gong, M. Paulose, K. G. Ong, E. C. Dickey, and C. A. Grimes, *Adv. Mater.* **15**, 624 (2003).
- [12] The term “band gap engineering”, introduced more than 30 years ago, generally refers to all attempts at modifying the band gap, e.g., by heterostructuring, combining suitable materials,

and doping.

- [13] V. Narayananamurti, Physics Today **37**(10), 24 (1984).
- [14] F. Capasso, Science **235**, 172 (1987).
- [15] Y. Q. Wang, G. Q. Hu, X. F. Duan, H. L. Sun, and Q. K. Xue, Chem. Phys. Lett. **365**, 427 (2002).
- [16] D. V. Potapenko, J. Hrbek, and R. M. Osgood, ACS Nano **2**, 1353 (2008).
- [17] J. Biener, E. Farfan-Arribas, M. Biener, C. M. Friend, and R. J. Madix, J. Chem. Phys. **123**, 094705 (2005).
- [18] B. Liu, J. E. Boercker, and E. S. Aydil, Nanotechnology **19**, 505604 (2008).
- [19] Y. J. Hwang, A. Boukai, and P. Yang, Nano Lett. **9**, 410 (2009).
- [20] P. Hoyer, Langmuir **12**, 1411 (1996).
- [21] S. P. Albu, A. Ghicov, J. M. Macak, R. Hahn, and P. Schmuki, Nano Lett. **7**, 1286 (2007).
- [22] G. K. Mor, K. Shankar, M. Paulose, O. K. Varghese, and C. A. Grimes, Nano Lett. **5**, 191 (2005).
- [23] G. K. Mor, O. K. Varghese, R. H. T. Wilke, S. Sharma, K. Shankar, T. J. Latempa, K. S. Choi, and C. A. Grimes, Nano Lett. **8**, 1906 (2008).
- [24] M. A. Khan and O. B. Yang, Catal. Today **146**, 177 (2009).
- [25] A. N. Enyashin and G. Seifert, Phys. Status Solidi (b) **242**, 1361 (2005).
- [26] A. M. Ferrari, D. Szieberth, M. Claudio, Z. Wilson, and R. Demichelis, J. Phys. Chem. Lett. **1**, 2854 (2010).
- [27] D. Szieberth, A. M. Ferrari, Y. Noel, and M. Ferrabone, Nanoscale **2**, 81 (2010).
- [28] R. A. Evarestov, A. V. Bandura, M. V. Losev, S. Piskunov, and Y. F. Zhukovskii, Physica E **43**, 266 (2010).
- [29] A. V. Bandura and R. A. Evarestov, Surf. Sci. **603**, L117 (2009).
- [30] O. K. Varghese, D. Gong, M. Paulose, C. A. Grimes, and E. C. Dickey, J. Mater. Res. **18**, 156 (2003).
- [31] F. Cesano, S. Bertarione, A. Damin, G. Agostini, S. Usseglio, J. G. Vitillo, C. Lamberti, G. Spoto, D. Scarano, and A. Zecchina, Adv. Mater. **20**, 3342 (2008).
- [32] G. Wang, H. Feng, L. Hu, W. Jin, Q. Hao, A. Gao, X. Peng, W. Li, K.-Y. Wong, H. Wang, Z. Li, and P. K. Chu, Nat. Comm. **9**, 2055 (2018).
- [33] D.-D. Qin, Q.H. Wang, J. Chen, C.-H. He, Y. Li, C.-H. Wang, J.-J. Quan, C.-L. Tao, and

X.-Q. Lu, *Sust. Energy Fuels* **1**, 248 (2017).

[34] Y. Yang, L. C. Kao, Y. Liu, K. Sun, H.o Yu, J. Guo, S. Y. H. Liou, and M. R. Hoffmann, *ACS Catal.* **8**, 4278 (2018).

[35] Z. Dong, D. Ding, T. Li, and C. Ning, *RSC Adv.* **8**, 5652 (2018).

[36] J. Li, X. Xu, X. Liu, C. Yu, D. Yan, Z. Sun, and L. Pan, *J. Alloys Comp.* **679**, 454 (2016).

[37] A. Chatzitakis, M. Grandcolas, K. Xu, S. Mei, J. Yang, I. J. T. Jensen, C. Simon, and T. Norby, *Catalysis Today* **287**, 161 (2017).

[38] D. J. Mowbray, J. I. Martinez, J. M. G. Lastra, K. S. Thygesen, and K. W. Jacobsen, *J. Phys. Chem. C* **113**, 12301 (2009).

[39] S. Piskunov, O. Lisovski, J. Begens, D. Bocharov, Y. F. Zhukovskii, M. Wessel, and E. Spohr, *J. Phys. Chem. C* **119**, 18686 (2015).

[40] A. Chesnokov, O. Lisovski, D. Bocharov, S. Piskunov, Y. F. Zhukovskii, M. Wessel, and E. Spohr, *Phys. Scr.* **90**, 094013 (2015).

[41] M. M. Fadlallah, *Physica E* **89**, 50 (2017).

[42] S.-M. Oh, S. S. Kim, J. E. Lee, T. Ishigaki, and D.-W. Park, *Thin Solid Films* **435**, 252 (2003).

[43] H. Ozaki, S. Iwamoto, and M. Inoue, *Chem. Lett.* **34**, 1082 (2005).

[44] R. Long, Y. Dai, G. Meng, and B. Huang, *Phys. Chem. Chem. Phys.* **11**, 8165 (2009).

[45] K. S. Yang, Y. Dai, and B. B. Huang, *Chem. Phys. Lett.* **456**, 71 (2008).

[46] Y. Duan, N. Fu, Q. Liu, Y. Fang, X. Zhou, J. Zhang, and Y. Lin, *J. Phys. Chem. C* **116**, 8888 (2012).

[47] M. Sun, X. Zhang, J. Li, X. Cui, D. Sun, and Y. Lin, *Electrochim. Commun.* **16**, 26 (2012).

[48] E. Arpaç, F. Sayılıkan, M. Asiltürk, P. Tatar, N. Kiraz, and H. Sayılıkan, *J. Hazardous Mater.* **140**, 69 (2007).

[49] J. Yu, J. C. Yu, B. Cheng, and X. Zhao, *J. Sol-Gel Sci. Techn.* **24**, 39 (2002).

[50] Y. J. Zhou, F. He, J. G. Qi, and Y. Wang, *Adv. Mater. Res.* **299-300**, 558 (2011).

[51] J. Xiao, Z. Pan, B. Zhang, G. Liu, H. Zhang, X. Song, G. Hu, C. Xiao, Z. Wei, and Y. Zheng, *Mater. Lett.* **188**, 66 (2017).

[52] Generally speaking, the accuracy of DFT-GGA calculations – which notoriously underestimate the band gap – is always an issue. In this context, we only wish to mention that this question is thoroughly discussed in a recent paper by Morales-García et al. [53], who conclude that

DFT-GGA is “an empirical, yet practical” approach. See also Refs. [63–65] in relation to the “scissors operation”.

- [53] Á. Morales-García, R. Valero, and F. Illas, *J. Phys. Chem. C* **121**, 18862 (2017).
- [54] J. P. Perdew, K. Burke, and M. Ernzerhof, *Phys. Rev. Lett.* **77**, 3865 (1996).
- [55] J. M. Soler, E. Artacho, J. D. Gale, A. García, J. Junquera, P. Ordejón, and D. Sánchez-Portal, *J. Phys.: Condens. Matter* **14**, 2745 (2002).
- [56] F. Nunzi and F. De Angelis, *J. Phys. Chem. C* **115**, 2179 (2011).
- [57] L. Deng, Y. Chen, M. Yao, S. Wang, B. Zhu, W. Huang, and S. Zhang, *J. Sol-Gel Sci. Technol.* **53**, 535 (2010).
- [58] Z. Zhao and Q. Liu, *J. Phys. D: Appl. Phys.* **41**, 085417 (2008).
- [59] C. G. V. de Walle and J. Neugebauer, *J. Appl. Phys.* **95**, 3851 (2004).
- [60] L. Kavan, M. Grätzel, S. E. Gilbert, C. Klemenz, and H. J. Scheel, *J. Am. Chem. Soc.* **118**, 6716 (1996).
- [61] Y. Su, S. Chen, X. Quan, H. Zhao, and Y. Zhang, *Appl. Surf. Sci.* **255**, 2167 (2008).
- [62] M. Bass, E. W. V. Stryland, D. R. Willians, and W. L. Woffe, *Handbook of Optics*, 2nd ed., vol. 1, McGraw-Hill, New York (1995).
- [63] H. Weng, J. Dong, T. Fukumura, M. Kawasaki, and Y. Kawazoe, *Phys. Rev. B* **73**, 121201 (2006).
- [64] F. H. Tian and C. B. Liu, *J. Phys. Chem. B* **110**, 17866 (2006).
- [65] X. Zhang, M. Guo, W. Li, and C. Liu, *J. Appl. Phys.* **103**, 063721 (2008).
- [66] X. Chen, S. Shen, L. Guo, and S. S. Mao, *Chem. Rev.* **110**, 6503 (2010).
- [67] B. Modak and S. K. Ghosh, *J. Phys. Chem. C* **119**, 23503 (2015).
- [68] Y. Xu and M. A. A. Schoonen, *Am. Mineral.* **85**, 543 (2000).